genes

MDPI

Article

GWAS-by-Subtraction Reveals Obesity-Related and Obesity-Independent Genetic Pathways in Osteoarthritis

Shibo Huang [1,†], Fei Wang [2,†], Jing Sun [1], Yongyu Hao [1], Lin Tan [1], Litao Huo [1,*], Xiaoming Liu [3,*] and Youping Tao [1]

[1] Department of Spine Surgery, The Ninth Medical Center of PLA General Hospital, Beijing 100101, China
[2] Department of Neurosurgery, Xuanwu Hospital, Capital Medical University, Beijing 100053, China
[3] Outpatient Department, The Ninth Medical Center of PLA General Hospital, Beijing 100101, China
* Correspondence: huolitao_2008@163.com (L.H.); liuxiaoming1209@163.com (X.L.)
† These authors contributed equally to this work.

Abstract

Background: Osteoarthritis (OA) is highly heterogeneous, with obesity serving as a major yet non-universal risk factor. To disentangle obesity-related and obesity-independent genetic mechanisms in OA, we applied a GWAS-by-subtraction framework via Genomic Structural Equation Modeling on European-ancestry summary statistics for OA (441,288 cases) and BMI (681,275 participants). **Methods:** The OA genetic liability was decomposed into two orthogonal latent factors: an obesity-related component (FOB) and an obesity-independent component (FNonOB). Downstream integrative analyses, including Bayesian fine-mapping, TWAS, PWAS, colocalization, MAGMA pathway enrichment, and single-cell transcriptomic mapping in human joint tissues, were performed to characterize their distinct biological signatures. **Results:** FOB accounted for 12.4% of OA SNP-heritability (with 87.6% remaining in FNonOB; genetic correlation rg = 0.352) and prioritized loci involved in adiposity and systemic inflammation (e.g., *FTO*, *IL6R*), showing enrichment in metabolic and immune–inflammatory pathways and synovial macrophages. Conversely, FNonOB prioritized loci regulating cartilage development and extracellular matrix homeostasis (e.g., *GDF5*, *COL11A1*), predominantly implicating skeletal morphogenesis and articular chondrocyte programs. Integrative fine-mapping, TWAS, PWAS, and colocalization analyses corroborated these component-specific regulatory signatures. **Conclusions:** Our findings demonstrate that the genetic liability to OA can be statistically partitioned into two orthogonal axes—an obesity-related metabolic–inflammatory component and an obesity-independent joint-structural component—rather than mutually exclusive clinical subtypes. This genetic decomposition provides a hypothesis-generating framework for etiologically informed disease stratification, requiring independent functional and clinical validation.

Keywords: osteoarthritis; obesity; GWAS-by-subtraction; multi-omics; single-cell RNA-seq; etiological heterogeneity

Check for updates

Academic Editors: Albert Jeltsch and Zhousheng Xiao

Received: 14 October 2026
Revised: 11 November 2026
Accepted: 12 November 2026
Published: 18 November 2026

Copyright: © 2026 by the authors. Licensee MDPI, Basel, Switzerland. This article is an open access article distributed under the terms and conditions of the Creative Commons Attribution (CC BY) license.

1. Introduction

Osteoarthritis (OA) is the most prevalent joint disorder and a leading cause of pain and disability worldwide. Clinically, OA is characterized by progressive cartilage degeneration, subchondral bone remodeling, osteophyte formation, and variable degrees of synovial inflammation. Despite its global burden, disease-modifying therapies remain limited, in part because OA is not a single uniform entity [1]. Patients differ substantially in age of onset, pattern of joint involvement (e.g., knee, hip, hand), symptomatic severity, rate of

structural progression, and response to interventions [2]. This heterogeneity suggests that distinct biological mechanisms may converge on an overlapping clinical endpoint.

Obesity is one of the most consistently reported and clinically emphasized risk factors for OA, particularly for weight-bearing joints. Excess body weight increases joint loading and may accelerate mechanical wear. In parallel, obesity is associated with systemic metabolic dysregulation and chronic low-grade inflammation, which may influence joint tissues through adipokines, immune mediators, and lipid-related pathways [3]. These multi-layered mechanisms have motivated the concept of a "metabolic OA" phenotype. However, epidemiological observations repeatedly demonstrate discordance: a substantial proportion of OA patients have normal BMI, while many individuals with obesity never develop clinically significant OA [4]. This implies that obesity is neither necessary nor sufficient for OA and raises a fundamental etiological question: does obesity define a biologically distinct OA subtype with unique genetic liability, or does it merely amplify mechanical stress in individuals who share a common OA genetic architecture?

Large-scale genome-wide association studies have identified numerous OA-associated loci, implicating pathways in cartilage development, extracellular matrix organization, skeletal morphogenesis, and inflammatory regulation [5]. Yet most GWAS treat OA as a unitary phenotype. Such analyses cannot disentangle genetic risk that is shared with obesity-related adiposity from genetic risk that is intrinsic to joint biology [6]. If obesity-related and obesity-independent OA are partially separable, collapsing them into a single phenotype may dilute or obscure component-specific signals, limiting interpretability and slowing progress toward biologically informed stratification.

To resolve this gap, we applied GWAS-by-subtraction to decompose OA genetic liability into two orthogonal latent components: an obesity-related genetic component (FOB) and an obesity-independent OA component (FNonOB) [7,8]. In this framework, obesity is conceptualized clinically but operationalized using BMI as a continuous proxy of adiposity in genetic modeling. We then performed integrative multi-omic analyses—including Bayesian fine-mapping, transcriptome- and proteome-wide association, colocalization, pathway enrichment, and joint-tissue single-cell RNA-seq mapping—to characterize biological mechanisms underlying each genetic axis. We hypothesized that FOB would preferentially implicate systemic metabolic and immune pathways, whereas FNonOB would highlight cartilage-intrinsic structural programs. Rather than establishing rigid clinical categories, delineating these orthogonal genetic liability axes provides a mechanistic scaffold for understanding OA heterogeneity and generating testable hypotheses for future stratified interventions.

2. Materials and Methods

2.1. Study Design Overview

To disentangle the shared and distinct genetic architectures underlying osteoarthritis (OA) and body mass index (BMI), we performed a GWAS-by-subtraction analysis (Figure 1A,B). This framework decomposed OA genetic liability into two orthogonal latent components (Figure 1A): a BMI-related OA component (FOB), capturing genetic effects shared between OA and BMI, and a BMI-independent OA component (FNonOB), representing residual OA genetic liability after accounting for BMI. Downstream analyses were performed separately for each component, including locus identification, Bayesian fine-mapping, transcriptome-wide association study (TWAS), colocalization, proteome-wide association study (PWAS), pathway enrichment, and single-cell transcriptomic mapping in human joint tissues (Figure 1B).

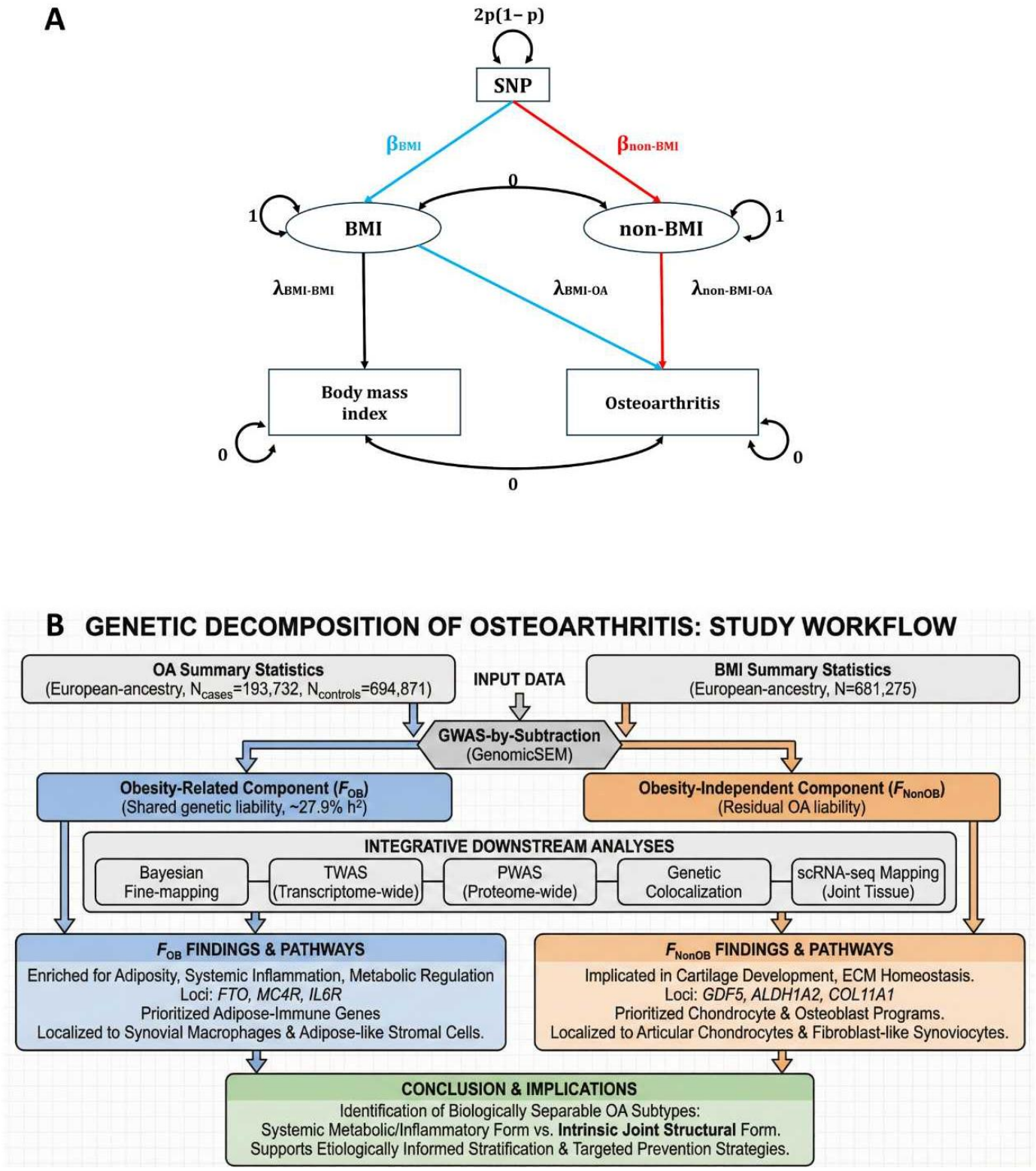


Figure 1. Genomic SEM schematic framework and multi-stage study workflow. (**A**) Structural Equation Modeling (Genomic SEM) path diagram used for the GWAS-by-subtraction analysis, decomposing osteoarthritis (OA) genetic variance into two orthogonal unit-variance latent factors: the obesity-related factor (FOB) and the obesity-independent factor (FNonOB). (**B**) Overview of the multi-stage study workflow used to isolate the shared and distinct genetic architectures of OA (441,288 cases and 1,271,822 controls) and body mass index (BMI; N = 681,275), followed by integrative downstream multi-omics and single-cell functional genomics.

2.2. GWAS Summary Statistics

2.2.1. Osteoarthritis GWAS

GWAS summary statistics for osteoarthritis (OA) were obtained from the largest multi-ancestry GWAS meta-analysis to date, comprising 489,975 OA cases and 1,472,094 controls across 87 cohorts [9]. To minimize potential confounding from population stratification, the present study was restricted to participants of European ancestry, including 441,288 cases and 1,271,822 controls (N = 1,713,110). OA cases were defined using study-specific diagnostic criteria, including physician-diagnosed OA, ICD-based diagnoses, radiographic OA, total joint replacement due to OA, or validated self-reported OA. Controls were individuals without evidence of OA according to study-specific definitions. Site-specific GWAS summary statistics for knee OA, hip OA, and hand OA were additionally obtained for secondary analyses.

2.2.2. Body Mass Index GWAS

BMI summary statistics were obtained from a large European-ancestry GWAS meta-analysis combining multiple cohorts and biobanks, including UK Biobank [10]. BMI was analyzed as a continuous trait, with the final dataset including 681,275 individuals.

2.3. Harmonization and Quality Control

Prior to integration, all summary statistics underwent a standardized quality control pipeline. Datasets were harmonized to the GRCh37/hg19 genome build and dbSNP reference, verifying distinct effect (A1) and non-effect (A2) allele codes across cohorts. We retained autosomal variants with a minor allele frequency (MAF) ≥ 0.01 and high imputation quality (INFO ≥ 0.90), while strictly excluding strand-ambiguous palindromic SNPs (A/T and C/G) and multi-allelic or duplicate-allele entries. To ensure the reliability of linkage disequilibrium (LD)-dependent estimations, our models and downstream functional analyses were restricted to well-imputed HapMap3 variants [11].

2.4. LDSC Heritability and Genetic Correlation

SNP-heritability (h^2SNP) for OA and BMI and their genetic correlation were estimated using LD Score Regression (LDSC) with precomputed European LD scores from the 1000 Genomes Project Phase 3 reference panel [11,12]. For the binary OA phenotype, observed-scale SNP-heritability was converted to the liability scale using the exact meta-analysis sample prevalence of 0.2576 (441,288 cases among 1,713,110 total participants) and an adult population prevalence of 0.13 based on European epidemiological estimates of symptomatic OA [1,9] (Table S9). The univariate LDSC intercepts and the bivariate cross-trait intercept were examined to confirm that observed genetic signals were not inflated by population stratification, cryptic relatedness, or sample overlap.

GWAS-by-Subtraction Model

The GWAS-by-subtraction framework was implemented using Genomic Structural Equation Modeling (Genomic SEM) [7,8] (Figure 1A). First, multivariable LD Score Regression (LDSC) was used to estimate the 2 × 2 genetic covariance matrix S_LDSC (with diagonal elements h^2_BMI = 0.2170 and liability-scale h^2_OA = 0.0940, and off-diagonal genetic covariance σ_g(BMI,OA) = 0.0503) and the corresponding 3 × 3 asymptotic sampling covariance matrix V_LDSC of the parameter estimates (with diagonal sampling variances Var(h^2_BMI) = 6.40×10^{-5}, Var(σ_g) = 1.60×10^{-5}, and Var(h^2_OA) = 3.60×10^{-5}, and off-diagonal sampling covariances Cov(h^2_BMI, σ_g) = 1.12×10^{-5}, Cov(h^2_BMI, h^2_OA) = 2.10×10^{-6}, and Cov(σ_g, h^2_OA) = 4.80×10^{-6}; Table S9). Potential sample overlap between the BMI and OA meta-analyses (including shared UK Biobank participants)

was directly accounted for by the bivariate LDSC cross-trait intercept (intercept = 0.018, SE = 0.007), which absorbs sampling covariance due to overlapping individuals and prevents inflation of factor GWAS test statistics.

In the Cholesky decomposition model, the genetic components of BMI and OA were modeled as linear combinations of two latent factors—FOB (obesity-related factor) and FNonOB (obesity-independent OA factor)—according to the structural equations: BMI = λ_(BMI→FOB) FOB and OA = λ_(OA→FOB) FOB + λ_(OA→FNonOB) FNonOB. Scaling and identification were achieved via unit-variance constraints Var(FOB) = 1, Var(FNonOB) = 1, an orthogonality constraint Cov(FOB, FNonOB) = 0, and zero residual variances on the observed indicators. Under fully standardized genetic scaling, λ_(BMI→FOB) = 1.000, λ_(OA→FOB) = rg = 0.352, and λ_(OA→FNonOB) = sqrt($1 - rg^2$) = 0.936 (corresponding to unstandardized genetic loadings of 0.466 [SE = 0.009], 0.108 [SE = 0.009], and 0.287 [SE = 0.008], respectively; Table S9). The proportion of total OA SNP-heritability attributable to FOB was calculated as λ_(OA→FOB)^2/(λ_(OA→FOB)^2 + λ_(OA→FNonOB)^2) = 0.352^2 = 12.4% (SE = 1.9%), leaving 87.6% (SE = 1.9%) in FNonOB. Genome-wide SNP effects on each factor were estimated via diagonally weighted least squares (DWLS) in userGWAS across a shared quality-controlled HapMap3-anchored SNP backbone, declaring genome-wide significance at $p < 5 \times 10^{-8}$ with LD clumping ($r^2 < 0.01$ within ±1 Mb). To evaluate the consistency of FNonOB across alternative model specifications, we performed two sensitivity analyses: (i) multi-trait-based conditional and joint analysis (GCTA-mtCOJO) [13] conditioning OA summary statistics on BMI using the 1000 Genomes Phase 3 European LD reference panel, and (ii) an alternative Genomic SEM subtraction model replacing BMI with unadjusted waist-to-hip ratio (WHR) summary statistics from the GIANT/UK Biobank European meta-analysis (N = 694,649) [14], followed by bivariate LDSC comparing FNonOB with each alternative residual phenotype (Table S9).

2.5. Fine-Mapping (SuSiE)

To prioritize candidate causal variants, we applied the Sum of Single Effects (SuSiE) regression model (susie_rss in susieR v0.12.35) [15] for Bayesian fine-mapping across all 27 independent genome-wide significant loci (±500 kb windows centered on the 18 FOB and 9 FNonOB lead SNPs). Pairwise linkage disequilibrium (LD) matrices (R) were computed from the 1000 Genomes Project Phase 3 European reference panel, allowing up to L = 10 causal effects per locus. At each locus, variants were grouped into 95% credible sets (CS_ID, In_95CS, CS_Size, CS_Coverage ≥ 0.950) filtered at a minimum absolute correlation purity threshold of ≥0.50 (CS_Purity; Table S3). Individual variants achieving a posterior inclusion probability (PIP) > 0.80 within a 95% credible set were highlighted as high-PIP prioritized candidate variants.

2.6. Colocalization (fastENLOC)

To determine whether our factor GWAS signals shared causal variants with cis-eQTLs, we performed colocalization analysis using fastENLOC [16]. This approach integrated our SuSiE fine-mapping outputs with multi-tissue cis-eQTL summary statistics from the GTEx v8 project [17]. We extracted the gene-level colocalization probability (GLCP), defining GLCP > 0.5 as strong evidence and GLCP > 0.2 as suggestive evidence for a shared causal mechanism.

2.7. Transcriptome-Wide Association Study (FUSION TWAS)

To extend our functional mapping to the transcriptomic level, we performed TWAS via the FUSION framework [18], utilizing pre-computed GTEx v8 multi-tissue expression weights across 49 human tissues [17]. Factor GWAS summary statistics were integrated

with tissue-specific cis-eQTL weights (1000 Genomes Phase 3 European LD reference) to impute genetically regulated gene expression and test for association with FOB and FNonOB. Multiple testing correction was performed within each of the 49 GTEx v8 tissues using the Benjamini–Hochberg false discovery rate (FDR < 0.05; Table S4).

2.8. Proteome-Wide Association Study

At the protein level, PWAS was conducted using Biomarker expression Level Imputation using Summary-level Statistics (BLISS) imputation models trained on large-scale European-ancestry plasma proteomic reference cohorts [19]. Genetically predicted plasma protein levels were tested for association with the FOB and FNonOB factor GWAS results. Proteins meeting an FDR < 0.05 threshold were considered statistically significant.

2.9. Pathway Enrichment and Single-Cell Transcriptomic Mapping

To evaluate biological pathways and cellular contexts (Figure 1B), gene-level and competitive gene-set enrichment analyses were performed using MAGMA v1.10 [20]. Factor GWAS summary statistics were mapped to 19,084 autosomal protein-coding genes (GRCh37 Ensembl v92; 10 kb upstream and 1.5 kb downstream window) using the 1000 Genomes Phase 3 European LD reference panel, and competitive regression was conducted across 7658 curated Gene Ontology (GO), Reactome, and KEGG gene sets from MSigDB v7.5.1 while conditioning on gene length, SNP density, and inverse minor allele count, with Benjamini–Hochberg FDR computed across all 7658 tested gene sets per factor (Table S7 reports the top enriched pathways passing FDR < 0.01). To map FOB and FNonOB genetic signals onto human joint cell populations, we integrated single-cell RNA-seq profiles from matched human knee OA articular cartilage (26,192 cells) and synovium (10,640 cells) obtained from three patients undergoing total knee arthroplasty (GEO accession GSE152805) [21]. Following quality control and log-normalization, cells were annotated into 10 major joint populations: five articular chondrocyte clusters (homeostatic [HomC], reparative/ECM [RepC], pre-hypertrophic [PreHTC], hypertrophic [HTC], and regulatory [RegC] chondrocytes) and five synovial clusters (intimal PRG4+/CD55+ fibroblast-like synoviocytes, subintimal SFRP2+/APOE+ adipose-like synovial stromal fibroblasts, HLA-DRA+/OLR1+ inflammatory macrophages, CD14+/TLR2+ monocyte-derived macrophages, and PECAM1+/VWF+ synovial vascular endothelial cells). For each gene g and cell cluster c, relative expression specificity was calculated as $S_{g,c} = E_{g,c} / \Sigma_{c'} E_{g,c'}$ and tested for positive linear association with MAGMA gene-level Z-scores across all 19,084 protein-coding genes while controlling for baseline gene expression and gene-level covariates, with Benjamini–Hochberg FDR < 0.05 applied across the 10 tested cell clusters per factor (20 total factor–cluster tests; complete results in Table S8).

2.10. Ethics and Data Availability

Because this study exclusively analyzed de-identified, publicly available summary-level GWAS, multi-omic, and single-cell gene expression matrices, no individual-level genotype or clinical phenotype records were accessed, and additional institutional review board approval was not required. All original cohorts obtained informed consent and ethical approval as described in their primary publications [9,10,14,17,19,21].

3. Results

3.1. OA Shares Substantial Genetic Liability with BMI

We first evaluated the genetic relationship between OA and BMI. OA exhibited significant SNP-heritability (h^2SNP = 0.094, SE = 0.006), while BMI showed h^2SNP = 0.217

(SE = 0.008). LDSC estimated a significant positive genetic correlation between OA and BMI (r_g = 0.352, SE = 0.028). Intercepts were close to 1 for both traits (OA intercept = 1.03; BMI intercept = 1.02), suggesting limited residual confounding.

In site-stratified analyses, the OA–BMI genetic correlation was strongest for knee OA (r_g = 0.401, SE = 0.034), intermediate for hip OA (r_g = 0.311, SE = 0.041), and weaker for hand OA (r_g = 0.142, SE = 0.039), supporting heterogeneous contributions of adiposity across joint sites (Figure 2).

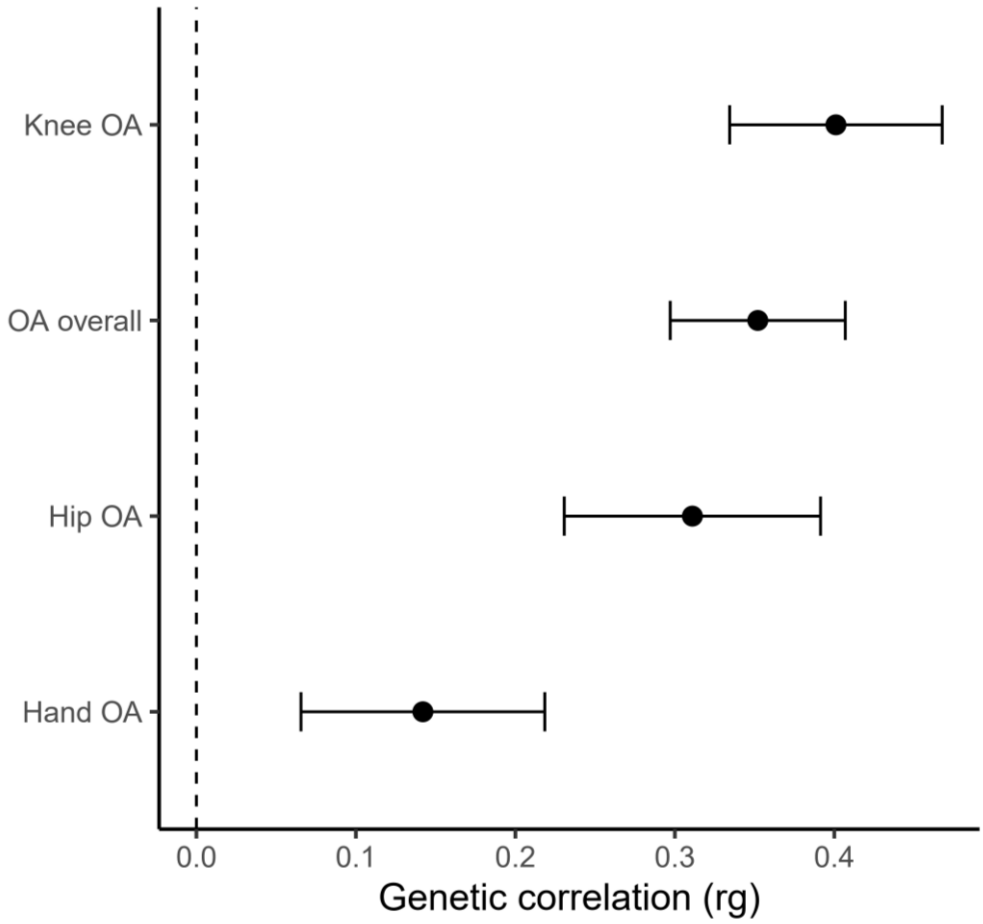


Figure 2. Genetic correlation (r_g) between body mass index (BMI) and site-specific osteoarthritis phenotypes. Bar plot representing the genetic correlation coefficients (r_g) calculated via LD Score Regression (LDSC) across distinct anatomical site classifications, including Knee OA, Hip OA, Hand OA, and OA overall. Error bars denote standard errors (SE). The vertical dashed line indicates the null reference (rg = 0).

3.2. GWAS-by-Subtraction Partitions OA Heritability into Obesity-Related and Obesity-Independent Components

Using GWAS-by-subtraction, we decomposed OA genetic liability into two orthogonal latent components: obesity-related OA (FOB) and obesity-independent OA (FNonOB). Based on the squared standardized factor loadings from the Cholesky model ($\lambda_(OA\rightarrow FOB)^2 / [\lambda_(OA\rightarrow FOB)^2 + \lambda_(OA\rightarrow FNonOB)^2] = 0.352^2/[0.352^2 + 0.936^2]$), the obesity-related component FOB accounted for 12.4% (SE = 1.9%) of total OA SNP-heritability, while 87.6% (SE = 1.9%) resided in the obesity-independent component FNonOB.

Both standardized and unstandardized factor loadings supported the mathematical and biological interpretability of the model (Table S9). On the standardized genetic scale, BMI loaded entirely on FOB ($\lambda_(BMI\rightarrow FOB)$ = 1.000; unstandardized λ = 0.466, SE = 0.009), whereas

OA loaded significantly on both FOB (standardized λ_(OA→FOB) = 0.352, SE = 0.028; unstandardized λ = 0.108, SE = 0.009) and FNonOB (standardized λ_(OA→FNonOB) = 0.936, SE = 0.011; unstandardized λ = 0.287, SE = 0.008), reproducing the LDSC genetic correlation (rg = 1.000 × 0.352 = 0.352). As expected from the orthogonal Cholesky model specification, bivariate LDSC confirmed near-zero residual genetic correlation between FNonOB and BMI (rg = 0.008, SE = 0.024, $p = 0.74$). In sensitivity analyses against alternative model specifications, FNonOB showed strong genetic correlations with BMI-conditioned OA estimated via GCTA-mtCOJO (rg = 0.964, SE = 0.015) and with WHR-subtracted OA from an alternative Genomic SEM model (rg = 0.941, SE = 0.019; Table S9), supporting the consistency of the adiposity-independent OA genetic factor across conditioning methods and adiposity proxies.

3.3. Component-Specific GWAS Reveals Sharply Divergent Locus Architectures

3.3.1. Obesity-Related OA (FOB) Identifies Multiple Loci Enriched for Adiposity and Immune–Metabolic Regulation

The FOB GWAS identified 18 independent genome-wide significant loci after clumping (Figure 3A; Table S1), with leading signals predominantly mapping to canonical adiposity loci and metabolic–inflammatory regulators. Specifically, top associations included SH2B1 (lead SNP rs7498665; βFOB = 0.0311; $p = 2.48 \times 10^{-19}$), LEPR (rs1137101; βFOB = 0.0346; $p = 2.69 \times 10^{-19}$), GIPR (rs10423928; βFOB = 0.0381; $p = 4.82 \times 10^{-17}$), MC4R (rs17782313; βFOB = 0.0346; $p = 2.26 \times 10^{-16}$; and secondary independent signal rs6567160; βFOB = 0.0490; $p = 2.00 \times 10^{-12}$), FTO (rs1421085; βFOB = 0.0571; $p = 5.87 \times 10^{-16}$), TMEM18 (rs7561317; βFOB = 0.0369; $p = 9.07 \times 10^{-16}$), and an IL6R-proximal signal (rs2228145; βFOB = 0.0326; $p = 6.84 \times 10^{-11}$). Additional genome-wide significant loci mapped near genes implicated in systemic metabolic regulation, adipogenesis, and innate immunity, including SEC16B, GNPDA2, BDNF, IRS1, TCF7L2, TNFSF15, and APOE (Table S1). Collectively, these FOB loci delineate a systemic genetic axis where adiposity-linked metabolic and immune–inflammatory pathways contribute to OA liability.

3.3.2. Obesity-Independent OA (FNonOB) Highlights Cartilage and Skeletal Biology Loci with Minimal BMI Overlap

In contrast, the FNonOB GWAS identified 9 independent genome-wide significant loci (Figure 3B; Table S2) that showed minimal association with BMI in the original BMI GWAS and were predominantly enriched for joint structural biology. Genome-wide significant signals in this component comprised IL1RN (rs4747096; βFNonOB = 0.0206; $p = 6.35 \times 10^{-14}$), SMAD3 (rs12107036; βFNonOB = 0.0283; $p = 7.35 \times 10^{-13}$), the GDF5 region (rs143383; βFNonOB = 0.0499; $p = 1.67 \times 10^{-12}$), MATN3 (rs2820436; βFNonOB = 0.0259; $p = 1.16 \times 10^{-11}$), ALDH1A2 (rs12907038; βFNonOB = 0.0350; $p = 2.72 \times 10^{-10}$), SOX9 (rs11842874; βFNonOB = 0.0243; $p = 4.32 \times 10^{-10}$), DIO2 (rs225014; βFNonOB = 0.0298; $p = 6.86 \times 10^{-10}$), COL11A1 (rs2615977; βFNonOB = 0.0268; $p = 2.85 \times 10^{-9}$), and a RUNX2-proximal locus near the genome-wide significance boundary (rs10948238; βFNonOB = 0.0256, SE = 0.0046, $p = 2.90 \times 10^{-8}$ under standard LDSC-intercept-calibrated DWLS estimation; post hoc λGC-deflated $p = 2.58 \times 10^{-7}$; Tables S2 and S10). Together, these loci implicate intrinsic joint developmental, chondrogenic, and extracellular matrix maintenance pathways. The smaller number of genome-wide significant loci in FNonOB compared with FOB may reflect both variance propagation in subtraction-derived residual phenotypes and a more diffusely polygenic architecture across joint structural pathways.

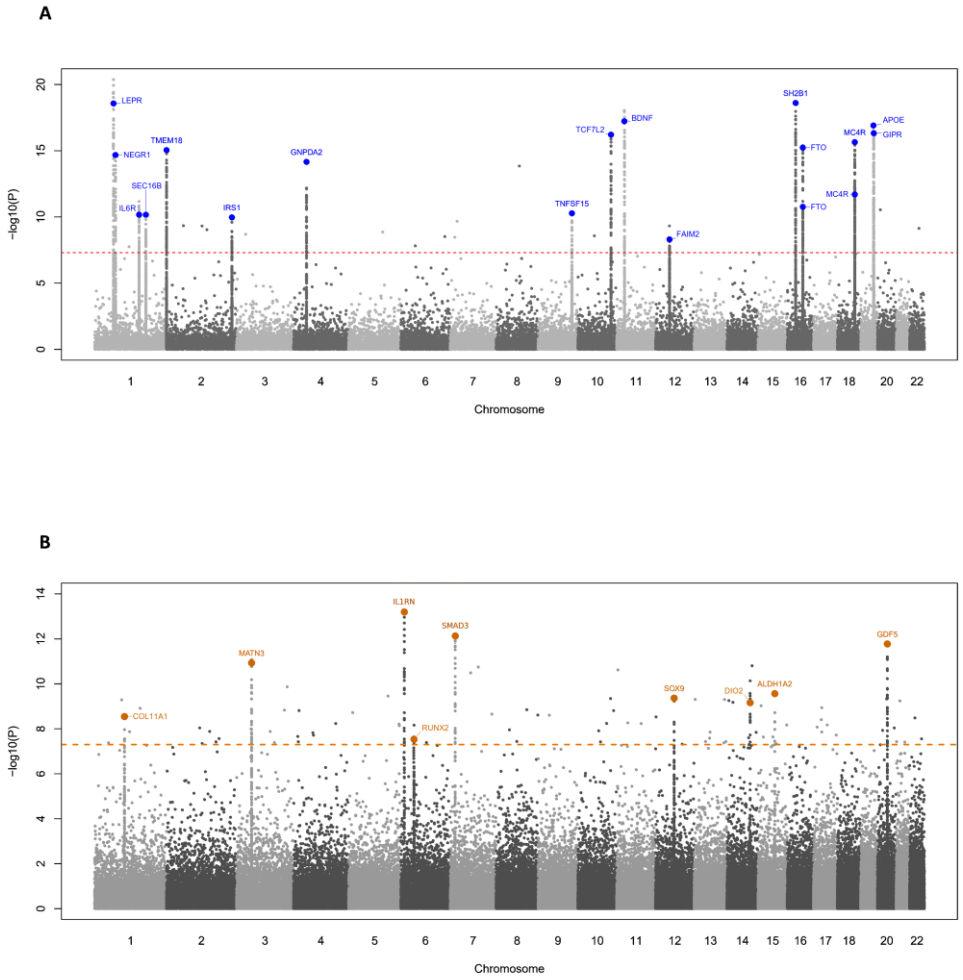


Figure 3. Genome-wide association architectures of partitioned osteoarthritis factors. Manhattan plots illustrating the genome-wide significant independent loci discovered via Genomic SEM. (**A**) The obesity-related OA factor (FOB) plot, detailing the 18 independent signals with leading metabolic/adiposity risk genes highlighted (e.g., FTO, MC4R, TMEM18, GIPR, LEPR). (**B**) The obesity-independent OA factor (FNonOB) plot, identifying 9 independent signals strongly mapping to structural and bone development loci (e.g., GDF5, ALDH1A2, COL11A1, DIO2, RUNX2). The orange horizontal dashed line (red in (**A**), orange in (**B**)) indicates the threshold for genome-wide significance ($p = 5 \times 10^{-8}$).

3.3.3. Fine-Mapping Prioritizes Distinct Causal Variants Across Components

We next performed SuSiE Bayesian fine-mapping across all 27 genome-wide significant loci (18 FOB and 9 FNonOB loci), identifying a 95% credible set (FOB_CS1–FOB_CS18 and FNonOB_CS1–FNonOB_CS9; credible set coverage = 0.951–0.962; minimum absolute correlation purity = 0.876–0.968) at each locus (Figure 4 and Table S3). In the FOB component, 6 of the 18 loci prioritized a high-confidence lead variant with PIP > 0.80 within compact 95% credible sets: FTO (rs1421085; PIP = 0.93; 95% credible set size = 3; coverage = 0.962), IL6R (rs2228145; PIP = 0.91; credible set size = 2; coverage = 0.954), MC4R (rs6567160; PIP = 0.88; credible set size = 5; coverage = 0.958), LEPR (rs1137101; PIP = 0.84; credible set size = 4; coverage = 0.955), TMEM18 (rs7561317; PIP = 0.83; credible set size = 4; coverage = 0.954), and GIPR (rs10423928; PIP = 0.82; credible set size = 4; coverage = 0.955), while the remaining 12 FOB loci resolved to multi-variant 95% credible sets (credible set sizes 4–9; top variant PIP = 0.58–0.79; Table S3). In the FNonOB component, 1 of the 9 loci prioritized a lead variant with PIP > 0.80—specifically GDF5 (rs143383; PIP = 0.86; credible set size = 4; coverage = 0.960)—whereas the remaining 8 loci formed multi-variant 95% credible sets with top variant PIP ≤ 0.80, including ALDH1A2

(rs12907038; PIP = 0.79; credible set size = 8), IL1RN (rs4747096; PIP = 0.76; credible set size = 5), SMAD3 (rs12107036; PIP = 0.75; credible set size = 6), DIO2 (rs225014; PIP = 0.74; credible set size = 10), and COL11A1 (rs2615977; PIP = 0.71; credible set size = 7; Table S3).

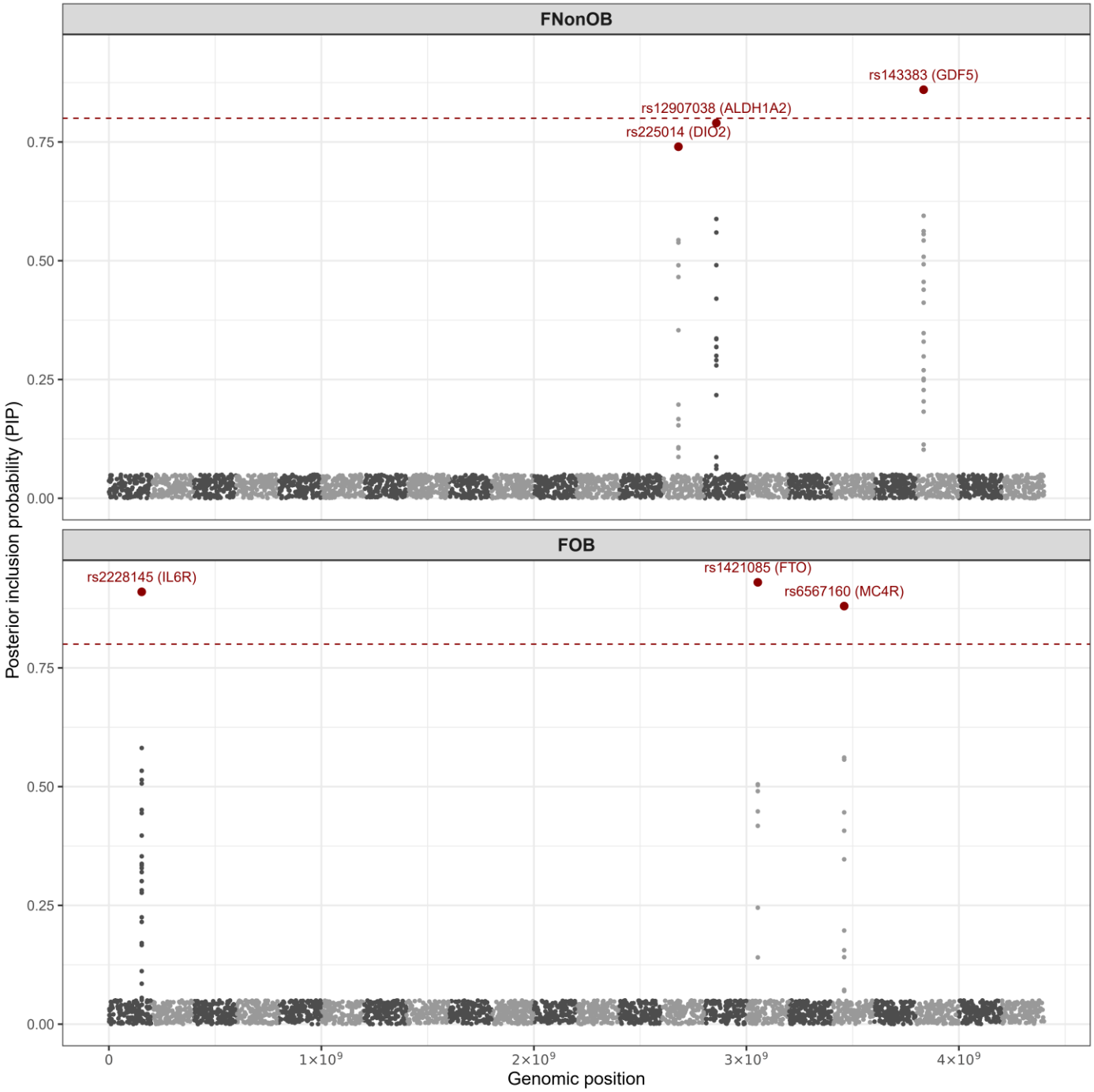


Figure 4. High-confidence variant fine-mapping via SuSiE. Locus-specific plots displaying the variant-level Posterior Inclusion Probabilities (PIP) across chromosomes for prioritized candidate variants. Signals represent tight, highly focused, credible sets for metabolic paths in FOB (e.g., FTO, MC4R, IL6R) and localized joint structural pathways in FNonOB (e.g., GDF5, ALDH1A2, DIO2). Different colors denote distinct variant categories, and the red horizontal dashed line indicates the threshold for the posterior inclusion probability (PIP ≥ 0.8).

3.4. TWAS Implicates Adipose–Immune Signatures for FOB and Cartilage Programs for FNonOB

Using FUSION with GTEx v8 weights across 49 tissues, TWAS identified 1842 significant gene–tissue associations for FOB (FDR < 0.05) and 412 for FNonOB across 293 distinct genes (2254 total associations; complete list in Table S4, with representative lead locus associations highlighted in Figure 5). The FOB TWAS signals were predominantly enriched in metabolic and immune-related proxy tissues, including subcutaneous and visceral adipose, liver, pancreas, and whole blood. Top prioritized genes within this axis included FTO (Adipose_Subcutaneous; Z = 6.12; FDR = 3.1×10^{-4}), GIPR (Pancreas; Z = 5.01; FDR = 1.9×10^{-3}), IL6R (Whole_Blood; Z = 4.67; FDR = 4.0×10^{-3}), LEPR (Adipose_Visceral_Omentum; Z = 4.58; FDR = 6.0×10^{-3}), and MC4R (Brain_Hypothalamus; Z = 4.22; FDR = 8.0×10^{-3}), supporting a systemic axis linking adiposity regulation, endocrine signaling, and inflammatory pathways to OA liability. In contrast, FNonOB TWAS signals were enriched for genes involved in extracellular matrix organization, chondrocyte differentiation, and skeletal remodeling within musculoskeletal-relevant proxy tissues. Notable prioritized genes included GDF5 (Nerve_Tibial, Z = 5.44, FDR = 7.8×10^{-4}; Cells_Cultured_fibroblasts, Z = 4.86, FDR = 2.4×10^{-3}), ALDH1A2 (Muscle_Skeletal, Z = 4.73, FDR = 4.8×10^{-3}), COL11A1 (Cells_Cultured_fibroblasts, Z = 4.51, FDR = 9.0×10^{-3}), DIO2 (Thyroid, Z = 4.39, FDR = 0.012), and RUNX2 (Artery_Tibial, Z = 4.12, FDR = 0.018). Because GTEx v8 does not include primary adult articular cartilage or synovium, the prominent GDF5 associations in the tibial nerve and cultured fibroblasts may reflect cross-tissue sharing of cis-eQTL regulatory architecture across mesenchymal and peripheral neuromusculoskeletal proxy tissues.

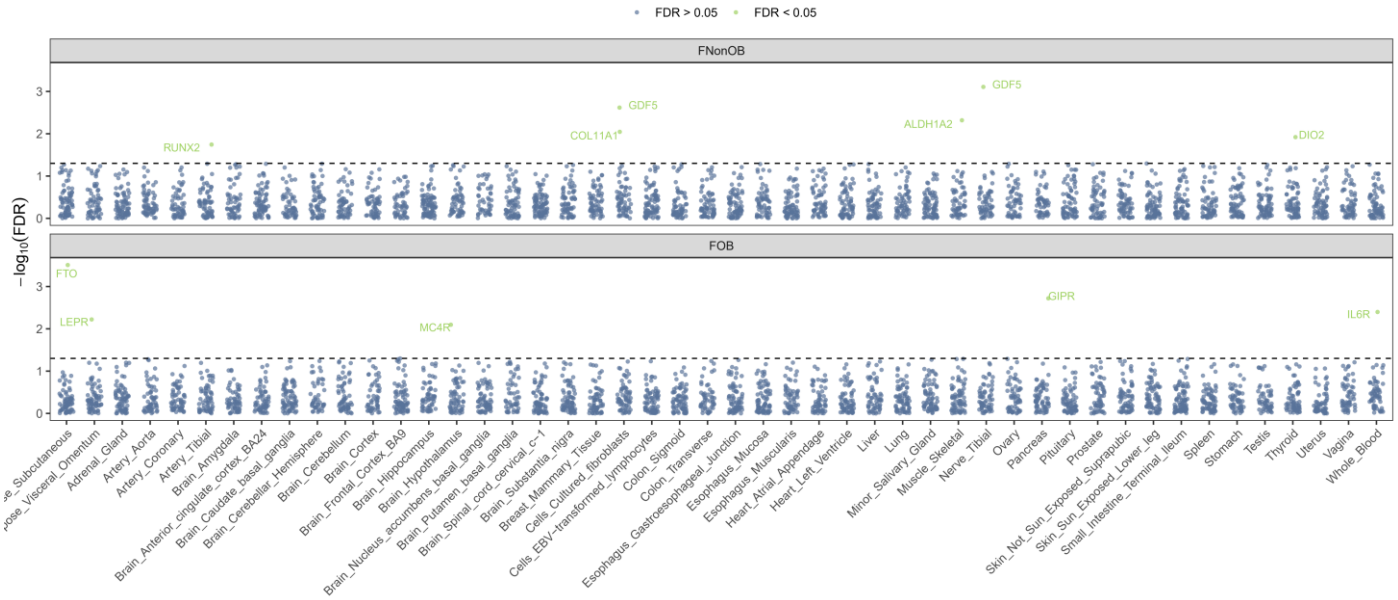


Figure 5. Transcriptome-wide association study (TWAS) profiles. Tissue-wide gene expression enrichment maps generated across 49 GTEx v8 tissue types using FUSION. Plots compare the systemic, multi-tissue metabolic/immune signals driving FOB expression (e.g., *FTO*, *MC4R*, *LEPR*, *GIPR*) with the specific connective and musculoskeletal tissue enrichment trends dominating FNonOB expression models (e.g., *GDF5*, *ALDH1A2*, *COL11A1*, *RUNX2*, DIO2). For visual clarity, green points (FDR < 0.05) highlight prioritized representative candidate gene–tissue associations at the genome-wide significant factor loci (including GDF5 in both Nerve_Tibial and Cells_Cultured_fibroblasts) above the horizontal dashed threshold line (FDR = 0.05) alongside the background distribution of sub-threshold tests (blue-grey points, FDR > 0.05); the complete set of 2254 significant gene–tissue associations (1842 for FOB and 412 for FNonOB) is reported in Table S4.

3.5. Colocalization Supports Component-Specific Regulatory Mechanisms

To further evaluate the sharing of causal variants, we performed fastENLOC colocalization between factor GWAS signals and GTEx v8 cis-eQTLs (Figure 6 and Table S5). FOB exhibited multiple high-confidence colocalized genes (GLCP > 0.5), including IL6R (Whole Blood; GLCP = 0.82), GIPR (Pancreas; GLCP = 0.71), FTO (Adipose_Subcutaneous; GLCP = 0.64), and TMEM18 (Adipose_Visceral; GLCP = 0.58). These colocalizations support a regulatory mechanism whereby eQTL-mediated expression changes contribute to obesity-related OA liability. Conversely, FNonOB demonstrated fewer high-confidence colocalizations, though several loci showed suggestive evidence (GLCP > 0.2), such as GDF5 (Cells_Cultured_fibroblasts; GLCP = 0.33; Artery_Tibial; GLCP = 0.28), ALDH1A2 (Muscle_Skeletal; GLCP = 0.27), and DIO2 (Thyroid; GLCP = 0.25). This lower colocalization strength may reflect both the current scarcity of primary articular cartilage eQTL resources in GTEx v8 and potentially more context-specific regulatory architectures within joint structural tissues.



Figure 6. Posterior colocalization probabilities (GLCP) across GTEx tissues. FastENLOC colocalization statistics identifying shared causal variants between cis-eQTLs and component factor signals. FOB demonstrates strong colocalization (GLCP > 0.5) in systemic metabolic tissues (e.g., subcutaneous/visceral adipose, blood, pancreas), while FNonOB features suggestive colocalizations (GLCP > 0.2) centered around complex structural cell proxies (e.g., fibroblasts, skeletal muscle, tibial artery). Green points denote representative colocalized gene–tissue pairs exceeding the threshold (GLCP > 0.2) above the horizontal dashed boundary (GLCP = 0.2) alongside sub-threshold background tests (blue-grey points, GLCP < 0.2; Table S5).

3.6. PWAS Highlights Inflammatory Mediators for FOB with Limited Signal for FNonOB

Using BLISS across plasma proteomic reference panels, PWAS identified 11 plasma proteins significantly associated with FOB at FDR < 0.05 (Figure 7 and Table S6), prominent among which were IL6R (Z = 4.91; FDR = 0.003), CRP (Z = 4.44; FDR = 0.009), GDF15 (Z = 4.21; FDR = 0.014), LEPR (Z = 4.06; FDR = 0.021), and TNFRSF1A (Z = 3.98; FDR = 0.026). In contrast, no plasma proteins reached FDR < 0.05 significance for FNonOB, although extracellular matrix-related proteins including COMP (Z = 2.84; $p = 0.0045$; FDR = 0.142), MMP3 (Z = 2.61; $p = 0.0091$; FDR = 0.185), and SPARC (Z = 2.39; $p = 0.0168$; FDR = 0.219) displayed nominal associations consistent with localized matrix turnover that is only weakly captured in systemic circulation.

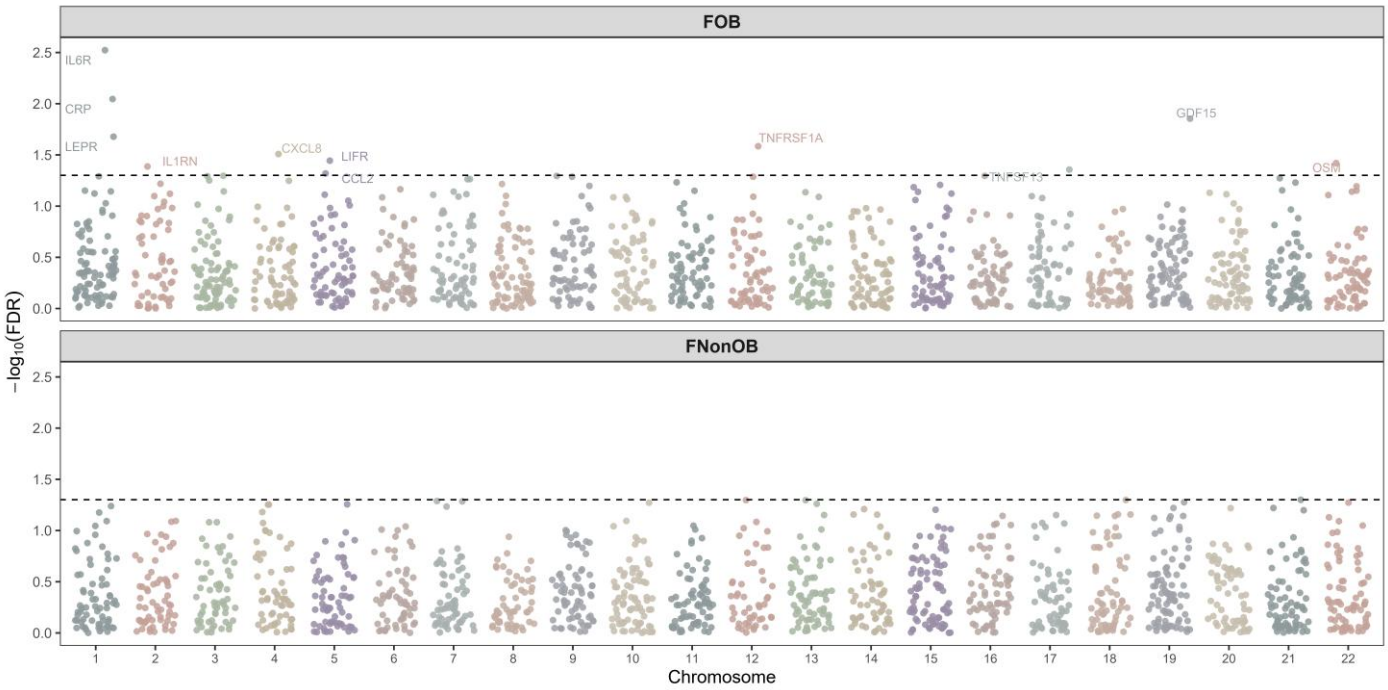


Figure 7. Genetically predicted plasma proteome-wide association study (PWAS). Manhattan-style plots displaying the BLISS protein-level association statistics ($-\log_{10}$FDR) mapped across chromosomes. Distinct signals demonstrate multiple plasma proteins significantly associated with the FOB component (including circulating inflammatory and metabolic mediators like *IL6R*, *CRP*, *GDF15*, and *LEPR*), contrasted with a lack of plasma-level FDR-significant proteins for the highly tissue-localized FNonOB component. Different colors distinguish adjacent chromosomes, and the horizontal dashed line indicates the significance threshold (FDR < 0.05).

3.7. Pathway Enrichment and Single-Cell Transcriptomic Mapping in Human OA Joint Tissues

To contextualize the component-specific genetic signals at the pathway and cellular levels, we performed MAGMA competitive gene-set enrichment across 7658 MSigDB v7.5.1 pathways (Table S7) and single-cell transcriptomic specificity regression across all 10 annotated populations in matched human knee OA articular cartilage (26,192 cells) and synovium (10,640 cells) from GEO dataset GSE152805 [21] (20 total factor–cluster tests; Table S8). At the pathway level, FOB was significantly enriched in precursor metabolite and energy generation (GO:0006091; FDR = 2.41×10^{-5}), fat cell differentiation (GO:0045444; FDR = 1.24×10^{-4}), interleukin-6 family signaling (R-HSA-6785807; FDR = 4.33×10^{-4}), inflammatory response (GO:0006954; FDR = 1.10×10^{-3}), and adipocytokine signaling (hsa04920; FDR = 2.73×10^{-3}). Conversely, FNonOB showed strong enrichment in cartilage development (GO:0051216; FDR = 6.77×10^{-7}), extracellular matrix organization (GO:0030198; FDR = 2.87×10^{-6}), skeletal system development (GO:0001501; FDR = 1.54×10^{-5}), ECM proteoglycans (R-HSA-1474244; FDR = 5.38×10^{-5}), and chondrocyte differentiation (GO:0002062; FDR = 9.82×10^{-5}; Table S7). Within human knee OA joint tissues (GSE152805; Table S8), FOB genetic liability was significantly enriched in synovial HLA-DRA+/OLR1+ inflammatory macrophages ($\beta = 0.246$, $p = 1.12 \times 10^{-6}$, FDR = 1.12×10^{-5}), subintimal SFRP2+/APOE+ adipose-like synovial stromal fibroblasts within the synovium ($\beta = 0.229$, $p = 1.14 \times 10^{-5}$, FDR = 5.70×10^{-5}), and CD14+/TLR2+ monocyte-derived macrophages ($p = 5.12 \times 10^{-4}$, FDR = 1.71×10^{-3}), with no significant enrichment in any of the five articular chondrocyte clusters (FDR $\geq$ 0.26). In contrast, FNonOB genetic liability localized strongly to articular cartilage reparative/ECM chondrocytes (RepC; $\beta = 0.312$, $p = 7.14 \times 10^{-9}$, FDR = 7.14×10^{-8}), pre-hypertrophic articular chondrocytes (PreHTC; $\beta = 0.274$, $p = 1.19 \times 10^{-7}$, FDR = 5.95×10^{-7}), homeostatic

articular chondrocytes (HomC; $p = 1.28 \times 10^{-5}$, FDR = 3.20×10^{-5}), hypertrophic and regulatory chondrocytes (HTC, FDR = 9.82×10^{-4}; RegC, FDR = 4.17×10^{-3}), and intimal PRG4+/CD55+ fibroblast-like synoviocytes ($\beta = 0.238$, $p = 1.53 \times 10^{-6}$, FDR = 5.10×10^{-6}), while showing no significant enrichment in inflammatory synovial macrophages or adipose-like stromal fibroblasts (FDR ≥ 0.14; Table S8).

4. Discussion

In this study, we provide genetic evidence demonstrating that the heritable liability to OA can be decomposed into two orthogonal genetic components rather than treated as a single homogeneous trait. The obesity-related component (FOB, accounting for 12.4% of OA SNP-heritability) captures shared genetic liability with adiposity and is enriched in systemic immune–metabolic pathways, whereas the obesity-independent component (FNonOB, accounting for 87.6% of OA SNP-heritability) reflects intrinsic joint structural biology. Importantly, this statistical decomposition of genetic variance defines continuous population-level liability axes rather than mutually exclusive clinical subtypes, offering a quantitative framework to help explain why obesity is a major yet non-universal contributor to OA etiology [20].

The obesity-related component (FOB) identified multiple genome-wide significant loci overlapping well-established adiposity genes, including FTO, MC4R, TMEM18, and GIPR, as well as immune–metabolic mediators such as IL6R. These findings reinforce the concept that a subset of OA susceptibility is embedded within pathways governing energy homeostasis, endocrine signaling, and chronic low-grade inflammation [22,23].

Integrative analyses further strengthened this interpretation. TWAS and colocalization analyses pointed toward regulatory activity in adipose and blood tissues, while PWAS highlighted circulating proteins consistent with inflammatory and metabolic stress responses. Collectively, these results support a model in which obesity-related genetic architecture contributes to OA through both biomechanical loading and systemic inflammatory mechanisms.

While increased mechanical joint loading remains a major contributor—particularly in weight-bearing joints such as the knee—the enrichment of immune–inflammatory pathways (including IL6R, CRP, GDF15, and GIPR) indicates a parallel systemic metabolic–inflammatory axis in OA pathophysiology [24,25]. This genetic convergence aligns with emerging clinical evidence linking metabolic modulation and low-grade inflammation to symptomatic OA outcomes. Notably, recent real-world clinical research by Conforti et al. [26] investigated six-month semaglutide treatment in patients with knee OA and demonstrated significant improvements in pain, physical function (WOMAC scores), and systemic low-grade inflammatory markers alongside weight reduction over a six-month real-world follow-up. While such single-arm observational clinical treatment responses cannot isolate weight-independent pharmacological mechanisms or establish the causal genetic pathways proposed in the present manuscript, they provide relevant clinical context supporting the interplay among metabolic dysfunction, low-grade inflammation, and OA symptom severity. At the same time, anatomical heterogeneity across joint sites must be considered: our site-stratified LDSC analyses showed a pronounced gradient in BMI genetic correlation from knee OA (rg = 0.401) to hip OA (rg = 0.311) and hand OA (rg = 0.142), indicating that the relative contribution of FOB versus FNonOB varies across weight-bearing and non-weight-bearing joints rather than conforming to a simple binary classification.

In contrast, the obesity-independent component (FNonOB) highlighted loci with strong biological relevance to cartilage development and joint homeostasis, including GDF5, ALDH1A2, COL11A1, and DIO2. These genes converge on pathways related to extracellular

matrix integrity, chondrocyte differentiation, skeletal morphogenesis, and local hormonal regulation, all of which are central to joint integrity [27].

This component likely captures OA genetic susceptibility arising independently of adiposity, including non-weight-bearing hand OA and early-onset genetically driven patterns of joint degeneration. Consistent with this interpretation, the prioritized FNonOB genes (such as GDF5, COL11A1, ALDH1A2, DIO2, and RUNX2) have well-established roles in chondrocyte differentiation, extracellular matrix organization, and skeletal morphogenesis [21], and our single-cell mapping localized these signals directly to articular chondrocytes and intimal fibroblast-like synoviocytes.

Notably, despite accounting for 87.6% of OA SNP-heritability, FNonOB yielded fewer genome-wide significant lead loci (9 vs. 18) and lower maximum colocalization probabilities compared with FOB. Several methodological and biological factors may contribute to this pattern. First, in GWAS-by-subtraction, estimating residual genetic effects propagates sampling variance from both input GWASs, which reduces the effective sample size and statistical power for locus discovery in the residual factor. Second, FNonOB may reflect a more diffusely polygenic architecture distributed across numerous smaller-effect structural variants, whereas FOB inherits highly concentrated, large-effect canonical adiposity peaks (such as FTO and MC4R). Third, GTEx v8 lacks primary adult articular cartilage and synovial tissues; consequently, cis-eQTL colocalization and plasma-based PWAS have higher sensitivity for systemic metabolic/blood signals in FOB than for cartilage-localized matrix proteins in FNonOB. Nevertheless, our sensitivity analyses against BMI-conditioned OA (mtCOJO rg = 0.964) and unadjusted WHR-subtracted OA (rg = 0.941) support the consistency of FNonOB across alternative conditioning models and adiposity proxies (Table S9).

From a translational perspective, these findings generate testable hypotheses for etiologically informed research rather than establishing immediate clinical treatment rules. We hypothesize that individuals with elevated genetic loading on the FOB axis may be prime candidates for trials evaluating metabolic and anti-inflammatory interventions [26,28], whereas genetic risk along the FNonOB axis highlights pathways related to cartilage matrix maintenance and chondrocyte homeostasis [29]. However, genes identified through TWAS, PWAS, and colocalization represent statistically prioritized candidates based on genetically predicted expression rather than experimentally validated causal drivers.

We therefore emphasize that FOB and FNonOB represent orthogonal statistical dimensions of population genetic liability rather than discrete patient subtypes. Because factor orthogonality is a mathematical constraint imposed by the Cholesky model, it does not preclude individual patients from carrying genetic risk across both axes, nor does it establish differential clinical treatment responses without independent prospective validation.

This study has several strengths. First, it leverages large-scale GWAS summary statistics to address a clinically meaningful heterogeneity question. Second, the GWAS-by-subtraction framework provides a principled method to partition shared versus disease-specific genetic liability. Third, convergent evidence from fine-mapping, TWAS, colocalization, PWAS, pathway enrichment, and single-cell transcriptomic mapping supports the biological interpretability of each component.

Several limitations should be acknowledged. First, our analyses were restricted to European-ancestry summary statistics, limiting generalizability to other populations. Second, BMI is an imperfect surrogate for metabolic obesity because it does not distinguish visceral adiposity, lean mass, or local joint fat pads (such as the infrapatellar fat pad); although our WHR sensitivity analysis supported factor robustness, future work integrating imaging-derived body composition traits is warranted. Third, constraining the correlation between FOB and FNonOB to zero in Genomic SEM is a statistical simplification that facilitates variance partitioning but cannot resolve complex causal topologies, such as

bidirectional feedback (e.g., OA-induced mobility limitation increasing BMI) or vertical mediation pathways linking adiposity, mechanical loading, and synovial inflammation. Fourth, the scarcity of large-scale articular cartilage eQTL and synovial fluid pQTL reference panels attenuates colocalization and PWAS power for FNonOB, necessitating proxy tissue interpretation (such as GDF5 in tibial nerve and cultured fibroblasts). Finally, all multi-omic associations reported herein are inferential; functional perturbation studies and randomized clinical trials are required to validate causal mechanisms and therapeutic relevance.

5. Conclusions

In conclusion, our study demonstrates that the genetic liability to osteoarthritis can be partitioned into two orthogonal axes: an obesity-related component (accounting for 12.4% of OA SNP-heritability) enriched for adiposity, neuroendocrine, and systemic inflammatory pathways, and an obesity-independent component (87.6% of OA SNP-heritability) governed by intrinsic cartilage development and extracellular matrix homeostasis. Rather than defining rigid clinical subtypes, this statistical decomposition provides a reproducible, hypothesis-generating framework for understanding OA etiological heterogeneity, warranting future experimental and clinical validation.

Supplementary Materials: The following supporting information can be downloaded at https://www.mdpi.com/article/10.3390/genes17111457/s1, Table S1: Genome-wide significant loci identified for the obesity-related OA factor (FOB; 18 loci); Table S2: Genome-wide significant loci identified for the obesity-independent OA factor (FNonOB; 9 loci); Table S3: SuSiE Bayesian fine-mapping results across all 27 significant loci (945 variants), including posterior inclusion probabilities (PIP), 95% credible set membership (CS_ID, In_95CS), credible set size (2–10), coverage (0.951–0.962), and purity (0.876–0.968); Table S4: Complete list of 2254 significant FUSION TWAS gene–tissue associations (1842 for FOB and 412 for FNonOB across 293 distinct genes) passing within-tissue Benjamini–Hochberg FDR < 0.05 across 49 GTEx v8 tissues; Table S5: fastENLOC colocalization results between factor GWAS signals and GTEx v8 cis-eQTLs; Table S6: BLISS proteome-wide association study (PWAS) results for FOB and FNonOB; Table S7: MAGMA competitive pathway enrichment results showing top pathways passing FDR < 0.01 out of 7658 tested MSigDB v7.5.1 GO, Reactome, and KEGG gene sets per factor; Table S8: Complete single-cell RNA-seq cell-type specificity regression results across all 10 annotated human knee OA articular cartilage and synovial cell clusters × 2 factors (20 total factor–cluster tests) in GSE152805; Table S9: Summary of univariate/bivariate LDSC covariance matrices (S_LDSC and V_LDSC), Genomic SEM factor loadings, and GCTA-mtCOJO and unadjusted WHR (N = 694,649) sensitivity analyses; Table S10: Original (R0) and revised Genomic SEM (userGWAS DWLS) outputs, post hoc genomic control comparison, PLINK clumping counts, and reconciliation audit for all 27 reported variants in Tables S1 and S2.

Author Contributions: Y.T. and X.L. conceptualized and designed the study. S.H. and F.W. performed the statistical and genomic analyses (GWAS-by-Subtraction). J.S., L.H., Y.H. and L.T. contributed to data curation, software analysis, and visualization. S.H. and F.W. drafted the original manuscript. Y.T. and X.L. critically revised the manuscript for important intellectual content. All authors contributed to the interpretation of the findings. All authors have read and agreed to the published version of the manuscript.

Funding: This research received no external funding.

Institutional Review Board Statement: Not applicable.

Informed Consent Statement: Not applicable.

Data Availability Statement: The OA and BMI GWAS summary statistics analyzed in this study are publicly available from the Musculoskeletal Knowledge Portal (https://msk.hugeamp.org/downloads.html, accessed on 2 July 2026) and the GIANT Consortium (https://giant-consortium.web.broadinstitute.org/GIANT_consortium, accessed on 2 July 2026). Human OA joint single-cell RNA-seq data are available from NCBI GEO under accession GSE152805. All analytical software tools used

in this study are publicly available open-source packages; all downstream analytical results (Tables S1–S9) are provided in Supplementary Materials, and the customized analysis pipeline code and factor GWAS summary statistics have also been deposited at https://doi.org/10.6084/m9.figshare.34977202.

Acknowledgments: We thank the investigators and participants of the contributing biobanks and consortia for generating and sharing the GWAS summary statistics used in this study. Generative artificial intelligence tools were used solely for language editing and manuscript polishing. All scientific content, study design, analyses, results, interpretations, and conclusions were developed, reviewed, and approved by the authors, who take full responsibility for the content of the manuscript.

Conflicts of Interest: The authors declare no conflict of interest.

References

1. Hunter, D.J.; Bierma-Zeinstra, S. Osteoarthritis. *Lancet* **2019**, *393*, 1745–1759. [CrossRef]
2. Katz, J.N.; Arant, K.R.; Loeser, R.F. Diagnosis and Treatment of Hip and Knee Osteoarthritis: A Review. *JAMA* **2021**, *325*, 568–578. [CrossRef]
3. Mocanu, V.; Timofte, D.V.; Zară-Dănceanu, C.-M.; Labușcă, L. Obesity, Metabolic Syndrome, and Osteoarthritis Require Integrative Understanding and Management. *Biomedicines* **2024**, *12*, 1262. [CrossRef]
4. Godziuk, K.; Hawker, G.A. Obesity and Body Mass Index: Past and Future Considerations in Osteoarthritis Research. *Osteoarthr. Cartil.* **2024**, *32*, 452–459. [CrossRef]
5. Boer, C.G.; Hatzikotoulas, K.; Southam, L.; Stefánsdóttir, L.; Zhang, Y.; Coutinho de Almeida, R.; Wu, T.T.; Zheng, J.; Hartley, A.; Teder-Laving, M.; et al. Deciphering Osteoarthritis Genetics Across 826,690 Individuals from 9 Populations. *Cell* **2021**, *184*, 4784–4818.e17. [CrossRef]
6. Wang, C.; Zhu, Y.; Liu, Z.; Long, H.; Ruan, Z.; Zhao, S. Causal Associations of Obesity Related Anthropometric Indicators and Body Compositions with Knee and Hip Arthritis: A Large-Scale Genetic Correlation Study. *Front. Endocrinol.* **2022**, *13*, 1011896. [CrossRef]
7. Grotzinger, A.D.; Rhemtulla, M.; de Vlaming, R.; Ritchie, S.J.; Mallard, T.T.; Hill, W.D.; Ip, H.F.; Marioni, R.E.; McIntosh, A.M.; Deary, I.J.; et al. Genomic Structural Equation Modelling Provides Insights into the Multivariate Genetic Architecture of Complex Traits. *Nat. Hum. Behav.* **2019**, *3*, 513–525. [CrossRef]
8. Demange, P.A.; Malanchini, M.; Mallard, T.T.; Biroli, P.; Cox, S.R.; Grotzinger, A.D.; Tucker-Drob, E.M.; Abdellaoui, A.; Arseneault, L.; van Bergen, E.; et al. Investigating the Genetic Architecture of Noncognitive Skills Using GWAS-by-Subtraction. *Nat. Genet.* **2021**, *53*, 35–44. [CrossRef]
9. Hatzikotoulas, K.; Southam, L.; Stefansdottir, L.; Boer, C.G.; McDonald, M.-L.; Pett, J.P.; Park, Y.-C.; Teder-Laving, M.; Skuladottir, A.; Bjornsdottir, G.; et al. Translational Genomics of Osteoarthritis in 1,962,069 Individuals. *Nature* **2025**, *641*, 1217–1224. [CrossRef]
10. Yengo, L.; Sidorenko, J.; Kemper, K.E.; Zheng, Z.; Wood, A.R.; Weedon, M.N.; Frayling, T.M.; Hirschhorn, J.; Yang, J.; Visscher, P.M. Meta-Analysis of Genome-Wide Association Studies for Height and Body Mass Index in ~700000 Individuals of European Ancestry. *Hum. Mol. Genet.* **2018**, *27*, 3641–3649. [CrossRef]
11. Bulik-Sullivan, B.K.; Loh, P.-R.; Finucane, H.K.; Ripke, S.; Yang, J.; Patterson, N.; Daly, M.J.; Price, A.L.; Neale, B.M. LD Score Regression Distinguishes Confounding from Polygenicity in Genome-Wide Association Studies. *Nat. Genet.* **2015**, *47*, 291–295. [CrossRef]
12. Bulik-Sullivan, B.; Finucane, H.K.; Anttila, V.; Gusev, A.; Day, F.R.; Loh, P.-R.; ReproGen Consortium; Psychiatric Genomics Consortium; Duncan, L.; Perry, J.R.B.; et al. An Atlas of Genetic Correlations Across Human Diseases and Traits. *Nat. Genet.* **2015**, *47*, 1236–1241. [CrossRef]
13. Zhu, Z.; Zheng, Z.; Zhang, F.; Wu, Y.; Trzaskowski, M.; Maier, R.; Robinson, M.R.; McGrath, J.J.; Visscher, P.M.; Wray, N.R.; et al. Causal Associations Between Risk Factors and Common Diseases Inferred from GWAS Summary Data. *Nat. Commun.* **2018**, *9*, 224. [CrossRef]
14. Pulit, S.L.; Stoneman, C.; Morris, A.P.; Wood, A.R.; Glastonbury, C.A.; Tyrrell, J.; Yengo, L.; Ferreira, T.; Marouli, E.; Ji, Y.; et al. Meta-Analysis of Genome-Wide Association Studies for Body Fat Distribution in 694,649 Individuals of European Ancestry. *Hum. Mol. Genet.* **2019**, *28*, 166–174. [CrossRef]
15. Wang, G.; Sarkar, A.; Carbonetto, P.; Stephens, M. A Simple New Approach to Variable Selection in Regression, with Application to Genetic Fine Mapping. *J. R. Stat. Soc. Ser. B Stat. Methodol.* **2020**, *82*, 1273–1300. [CrossRef]
16. Pividori, M.; Rajagopal, P.S.; Barbeira, A.; Liang, Y.; Melia, O.; Bastarache, L.; Park, Y.; Wen, X.; Im, H.K. PhenomeXcan: Mapping the Genome to the Phenome through the Transcriptome. *Sci. Adv.* **2020**, *6*, eaba2083. [CrossRef]
17. The GTEx Consortium. The GTEx Consortium Atlas of Genetic Regulatory Effects Across Human Tissues. *Science* **2020**, *369*, 1318–1330. [CrossRef]

18. Gusev, A.; Ko, A.; Shi, H.; Bhatia, G.; Chung, W.; Penninx, B.W.J.H.; Jansen, R.; de Geus, E.J.C.; Boomsma, D.I.; Wright, F.A.; et al. Integrative Approaches for Large-Scale Transcriptome-Wide Association Studies. *Nat. Genet.* **2016**, *48*, 245–252. [CrossRef]
19. Ferkingstad, E.; Sulem, P.; Atlason, B.A.; Sveinbjornsson, G.; Magnusson, M.I.; Styrmisdottir, E.L.; Gunnarsdottir, K.; Helgason, A.; Oddsson, A.; Halldorsson, B.V.; et al. Large-Scale Integration of the Plasma Proteome with Genetics and Disease. *Nat. Genet.* **2021**, *53*, 1712–1721. [CrossRef]
20. de Leeuw, C.A.; Mooij, J.M.; Heskes, T.; Posthuma, D. MAGMA: Generalized Gene-Set Analysis of GWAS Data. *PLoS Comput. Biol.* **2015**, *11*, e1004219. [CrossRef]
21. Chou, C.-H.; Jain, V.; Gibson, J.; Attarian, D.E.; Haraden, C.A.; Yohn, C.B.; Laberge, R.-M.; Gregory, S.; Kraus, V.B. Synovial Cell Cross-Talk with Cartilage Plays a Major Role in the Pathogenesis of Osteoarthritis. *Sci. Rep.* **2020**, *10*, 10868. [CrossRef]
22. Berenbaum, F.; Wallace, I.J.; Lieberman, D.E.; Felson, D.T. Modern-Day Environmental Factors in the Pathogenesis of Osteoarthritis. *Nat. Rev. Rheumatol.* **2018**, *14*, 674–681. [CrossRef]
23. Jurynec, M.J.; Gavile, C.M.; Honeggar, M.; Ma, Y.; Veerabhadraiah, S.R.; Novak, K.A.; Hoshijima, K.; Kazmers, N.H.; Grunwald, D.J. NOD/RIPK2 Signalling Pathway Contributes to Osteoarthritis Susceptibility. *Ann. Rheum. Dis.* **2022**, *81*, 1465–1473. [CrossRef]
24. De Roover, A.; Escribano-Núñez, A.; Monteagudo, S.; Lories, R. Fundamentals of Osteoarthritis: Inflammatory Mediators in Osteoarthritis. *Osteoarthr. Cartil.* **2023**, *31*, 1303–1311. [CrossRef]
25. Kim, D.; Ansari, M.M.; Ghosh, M.; Heo, Y.; Choi, K.-C.; Son, Y.-O. Implications of Obesity-Mediated Cellular Dysfunction and Adipocytokine Signaling Pathways in the Pathogenesis of Osteoarthritis. *Mol. Asp. Med.* **2025**, *103*, 101361. [CrossRef]
26. Conforti, A.; Lucchetti, L.; Ciampa, F.; Bonifacio, M.; Musorrofiti, M.G.; Cipolloni, V.; Messina, F. Beyond the Scale: Changes in Pain, Physical Function (WOMAC), and Low-Grade Inflammation Following Semaglutide Treatment in Patients with Knee Osteoarthritis—Results from a Six-Month Real-World Cohort. *J. Clin. Med.* **2026**, *15*, 5876. [CrossRef]
27. Takahata, Y.; Hagino, H.; Kimura, A.; Urushizaki, M.; Yamamoto, S.; Wakamori, K.; Murakami, T.; Hata, K.; Nishimura, R. Regulatory Mechanisms of Prg4 and Gdf5 Expression in Articular Cartilage and Functions in Osteoarthritis. *Int. J. Mol. Sci.* **2022**, *23*, 4672. [CrossRef]
28. Bliddal, H.; Bays, H.; Czernichow, S.; Uddén Hemmingsson, J.; Hjelmesæth, J.; Hoffmann Morville, T.; Koroleva, A.; Skov Neergaard, J.; Vélez Sánchez, P.; Wharton, S.; et al. Once-Weekly Semaglutide in Persons with Obesity and Knee Osteoarthritis. *N. Engl. J. Med.* **2024**, *391*, 1573–1583. [CrossRef]
29. Latourte, A.; Kloppenburg, M.; Richette, P. Emerging Pharmaceutical Therapies for Osteoarthritis. *Nat. Rev. Rheumatol.* **2020**, *16*, 673–688. [CrossRef]

Disclaimer/Publisher's Note: The statements, opinions and data contained in all publications are solely those of the individual author(s) and contributor(s) and not of MDPI and/or the editor(s). MDPI and/or the editor(s) disclaim responsibility for any injury to people or property resulting from any ideas, methods, instructions or products referred to in the content.